


NANO EXPRESS

Open Access



Bi₂Se₃ Sensitized TiO₂ Nanotube Films for Photogenerated Cathodic Protection of 304 Stainless Steel Under Visible Light

Wencheng Wang^{1,2,3}, Xiutong Wang^{1,2,5*} , Ning Wang^{1,3}, Xiaobo Ning², Hong Li⁴, Dongzhu Lu¹, Xiangju Liu^{1,3}, Qichao Zhang^{1,3} and Yanliang Huang^{1,2,5*}

Abstract

Titanium dioxide (TiO₂) nanotube arrays coupled with a narrow gap semiconductor—bismuth selenide (Bi₂Se₃)—exhibited remarkable enhancement in the photocathodic protection property for 304 stainless steel under visible light. Bi₂Se₃/TiO₂ nanocomposites were successfully synthesized using a simple two-step method, including an electrochemical anodization method for preparing pure TiO₂ and a chemical bath deposition method for synthesizing Bi₂Se₃ nanoflowers. The morphology and structure of the composite films were studied by scanning electron microscopy, energy dispersion spectroscopy, X-ray photoelectron spectroscopy and X-ray diffraction. In addition, the influence of the Bi₂Se₃ content on the photoelectrochemical and photocathodic protection properties of the composite films was also studied. The photocurrent density of the Bi₂Se₃/TiO₂ nanocomposites was significantly higher than that of pure TiO₂ under visible light. The sensitizer Bi₂Se₃ enhanced the efficient separation of the photogenerated electron-hole pairs and the photocathodic protection properties of TiO₂. Under visible light illumination, Bi₂Se₃/TiO₂ nanocomposites synthesized by the chemical bath deposition method with Bi³⁺ (0.5 mmol/L) exhibited the optimal photogenerated cathodic protection performance for 304 stainless steel.

Keywords: TiO₂, Bi₂Se₃, Stainless steel, Heterojunction, Photocathodic protection

Background

As important engineering materials, stainless steels have been widely applied to significant projects in numerous fields due to their excellent corrosion resistance. However, stainless steels can suffer serious corrosion when used in specific aggressive environments, such as acid environments, as well as under chloride-containing or high-temperature conditions [1–4]. Extensive research and applications of the traditional anti-corrosion method, including coatings [5, 6], use of a sacrificial anode [7] and impressed current cathodic protection [8, 9], have been developed during the past few decades. However, eco-friendly and long-lasting anticorrosion technology still remains a major objective. As a new anti-corrosion technology, photocathodic protection was first proposed by

Yuan and Tsujikawa in 1995 [10] before receiving attention from corrosion researchers [11–14].

Titanium dioxide (TiO₂) is an important photoelectric material with good photoelectric conversion and photocatalysis properties and is widely used in catalysts [15], solar cells [16] and gas sensors [17] due to its low cost, non-toxicity and stable chemical properties. TiO₂ and TiO₂-based composites are used for photogenerated cathodic protection: a promising technique for corrosion prevention that has undergone rapid development in recent years [18–23]. However, the bandgap (3.2 eV) of TiO₂ restricts the photoresponse to only the ultraviolet region, which significantly depresses the utilization ratio of solar power. In addition, photo-induced charge carriers in bare TiO₂ nanoparticles show a very short lifetime due to the rapid recombination of photo-excited electron-hole pairs, which reduces the photocathodic protection effect of pure TiO₂ films. Thus, how to overcome the above deficiencies of TiO₂ has become a widely studied topic. Many studies have been conducted on compounding TiO₂ with

* Correspondence: wangxiutong@qdio.ac.cn; hyl@qdio.ac.cn

¹Key Laboratory of Marine Environmental Corrosion and Bio-fouling, Institute of Oceanology, Chinese Academy of Sciences, 7 Nanhai Road, Qingdao 266071, China

Full list of author information is available at the end of the article

non-metal elements (F, N and S) [12, 24, 25], metal atoms (Fe, Co, Cu and Ce) [26–29] and some narrow bandgap nano-semiconductors (Ag_2O , ZnSe , WO_3 , CdS , Ag_2S , CdSe and Bi_2S_3) [30–36] to improve the carrier separation and light utilization of TiO_2 .

Bismuth selenide (Bi_2Se_3) is a direct bandgap layered semiconductor and important member of the V_2VI_3 compound family. It has a high absorption coefficient in the visible and near-infrared light regions with a narrow bandgap (0.35 eV) [37]. As an important n-type chalcogenide, Bi_2Se_3 possesses many important characteristics, such as a high electrical conductivity [38], appreciable thermoelectric property [39], photosensitivity [40], electrochemical property [41] and photoconductivity [42]. Furthermore, Bi_2Se_3 is a popular topological insulator [43–45] and has the unique property of conductive surface states and insulated bulk states. High-quality Bi_2Se_3 nanostructures have been prepared using a high vacuum physical deposition method, chemical vapour deposition, atomic layer deposition, pulsed laser deposition and a vapour-liquid-solid technique at high temperature [44–49]. These synthetic methods for Bi_2Se_3 require a difficult fabrication, leading to a high production cost. In this paper, the above problems are overcome by employing a low-cost and simple chemical bath deposition method for Bi_2Se_3 nanoflower deposition on TiO_2 . The combination of a n- Bi_2Se_3 /n- TiO_2 heterojunction as an efficient photoanode was applied to the photogenerated cathodic protection of 304ss for the first time. The morphology, structure and optical absorption property of $\text{Bi}_2\text{Se}_3/\text{TiO}_2$ nanocomposites were studied by scanning electron microscopy (SEM), X-ray diffraction (XRD), energy-dispersive X-ray spectroscopy (EDS), X-ray photoelectron spectroscopy (XPS) and UV-visible (UV-Vis) diffuse reflectance spectra, respectively.

Methods

All of the chemicals used in this study were of analytical grade and used as received without further purification. All of the aqueous solutions were prepared using deionized water.

Preparation of TiO_2 Film

Ti foils (20 mm \times 10 mm \times 0.3 mm; > 99.9% purity) were polished using a mixture containing NH_4F (2.25 g), H_2O (12.5 mL), H_2O_2 (30 wt%, 30 mL) and HNO_3 (68 wt%, 30 mL), and then, Ti pieces were cleaned with deionized water and ethanol. TiO_2 film was prepared on Ti foil by the anodic oxidation method reported in the literature [50]. The Pt plate was chosen as the cathode, and the Ti foil was the anode at 20 V for 1 h in an ethylene glycol solution containing NH_4F (0.22 g), H_2O (4 mL) and ethylene glycol (40 mL) at ambient temperature. After that, the samples were rinsed with deionized water and ethanol. Finally, the specimens were

annealed at 450 °C for 2 h and cooled in ambient air to obtain TiO_2 film.

Synthesis of Bi_2Se_3 on the TiO_2 Film

The Bi_2Se_3 was prepared by the chemical bath deposition method. In the experimental procedure, 8 mmol of nitrilotriacetic acid (H_3NTA) and 0.4 mmol of $\text{Bi}(\text{NO}_3)_3 \cdot 5\text{H}_2\text{O}$ were added to deionized water (400 mL) to form the bismuth chelate, with a Bi^{3+} concentration of 1.0 mmol/L in the mixed solution. Two millimoles of ascorbic acid as the reducing reagent was added to the above solution, and then, ammonium hydroxide was cautiously added, dropwise, until the pH of the mixture was adjusted to approximately 8.6–8.9 and mixed solution appeared colourless and transparent. Finally, Na_2SeSO_3 (20 mL, 30 mmol/L) was injected into the above solution. In all of the above experiments, the aqueous solutions were thoroughly stirred with a magnetic stirrer to obtain a homogeneous solution. Then, a TiO_2 substrate was immersed in the final solution (40 mL) in a beaker (100 mL). The beaker covered with cling film was then transferred into an oven heated to a temperature of 80 °C for 200 min to obtain the Bi_2Se_3 nanoflower on the TiO_2 substrate. Finally, the sample was removed from the beaker and washed several times with deionized water and ethanol and then allowed to dry in ambient air. In this way, Bi_2Se_3 -sensitized TiO_2 films were obtained and labelled with $\text{Bi}_2\text{Se}_3/\text{TiO}_2$ -1.0. For simplicity, different quantities of Bi_2Se_3 on TiO_2 substrates are designated as $\text{Bi}_2\text{Se}_3/\text{TiO}_2$ - γ in this paper, where γ denotes the concentration of Bi^{3+} in the H_3NTA and $\text{Bi}(\text{NO}_3)_3 \cdot 5\text{H}_2\text{O}$ solution. With the quantities of the other reagents held constant, $\text{Bi}_2\text{Se}_3/\text{TiO}_2$ -0.5 and $\text{Bi}_2\text{Se}_3/\text{TiO}_2$ -0.25 were obtained for Bi^{3+} concentrations of 0.5 mmol/L and 0.25 mmol/L, respectively. The influence of different quantities of Bi_2Se_3 on the photoelectrochemical and photocathodic protection properties of the composite films was investigated in this paper.

Morphology and Composition Analysis

Scanning electron microscopy (SEM, Hitachi S-4800, Japan) was used to investigate the morphologies of the prepared films. Energy-dispersive X-ray spectroscopy (EDS, Oxford Energy 350 X-ray energy spectrum analyser) and X-ray photoelectron spectroscopy (XPS, Thermo Scientific ESCALAB 250Xi) were employed to determine the chemical composition of the $\text{Bi}_2\text{Se}_3/\text{TiO}_2$ nanocomposites. UV-Vis DRS (Japan Hitachi UH4150) was used to determine the light absorbance of the samples. The crystalline phase composition of the samples was characterised by an X-ray diffractometer (XRD, Germany Bruker AXSD8) using Cu K_α radiation ($\lambda = 1.54056 \text{ \AA}$) from 10° to 80°.

Photoelectrochemical Measurements

As shown in Fig. 1, a coupling system comprising photolysis and electrolytic cells was used for the photoelectrochemical measurements, and a proton exchange membrane was used to link the two cells together. The photolysis cell contained a 0.1 mol/L Na_2S and 0.2 mol/L NaOH mixed solution, which played the role of a sacrificial agent for promoting the separation of electrons and holes [33, 51], while a 0.5 mol/L NaCl solution was used as the electrolyte for the electrolytic cell. In the electrolytic cell, a three-electrode system was adopted with a Pt foil as the counter electrode (CE), saturated calomel electrode as the reference electrode (RE) and 304ss as the working electrode (WE). $\text{Bi}_2\text{Se}_3/\text{TiO}_2$ nanocomposite samples placed in the photolysis cell were connected to a 304ss electrode immersed in the electrolytic cell by a copper wire. The light source in the visible light range was irradiated by a high-pressure xenon lamp (PLS-SXE 300 C, Beijing Perfectlight Company, China). The changes in the open-circuit potential (OCP) and photocurrent curves were measured using a Gamry potentiostat/galvanostat/ZRA system (GAMRY 3000, Gamry Instruments, USA) before and during light irradiation.

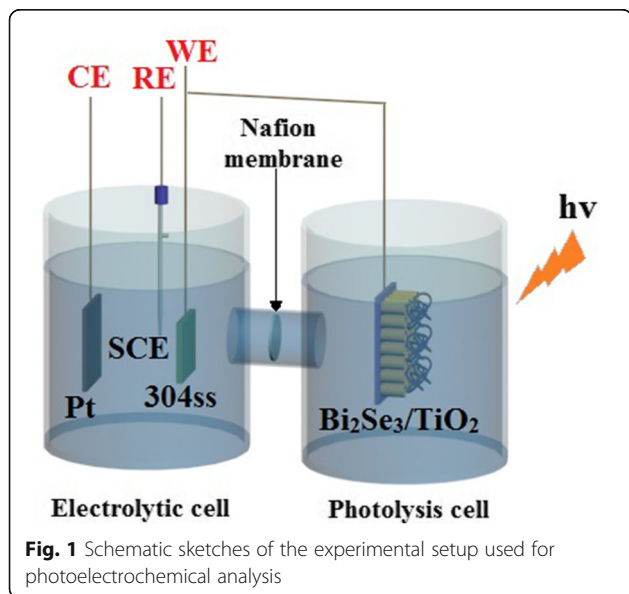
Results and Discussion

Characterization of Pure TiO_2 and $\text{Bi}_2\text{Se}_3/\text{TiO}_2$

Figure 2a shows typical top view and cross-sectional topographies for TiO_2 films prepared under the anodization method. The TiO_2 nanotube arrays show a nanoporous structure composed of well-ordered and high-density nanotubes with an average inner diameter and length of approximately 55 nm and 680 nm, respectively. As shown in Fig. 2b–d, the TiO_2 nanotube surfaces were successfully

modified by Bi_2Se_3 via the chemical bath deposition method for different concentrations of Bi^{3+} . For $\text{Bi}_2\text{Se}_3/\text{TiO}_2$ -0.25, the Bi_2Se_3 nanoflakes were sporadically distributed and aggregated unevenly across the TiO_2 nanotubes (Fig. 2b). When the concentration of Bi^{3+} was 0.5 mmol/L, Bi_2Se_3 was composed almost entirely of flower-like patterns of pliable ultrathin nanoflakes with a diameter of approximately 800 nm, without blocking the nozzle of the TiO_2 nanotubes or damaging them (Fig. 2c). Bi_2Se_3 nanoflowers that were observed to be evenly distributed on the surface of the TiO_2 showed an internal cross-linked structure for the ultrathin nanoflakes, which effectively prevented lamella aggregation and maintained a long-standing lifetime of the architectures, as shown in Fig. 2c. After the concentration of Bi^{3+} was increased to 1.0 mmol/L, the amount and diameter of the Bi_2Se_3 nanoflowers significantly increased, and the agglomeration of nanoflowers blocked the nanotubes, as shown in Fig. 2d. The corresponding EDS spectrum of the $\text{Bi}_2\text{Se}_3/\text{TiO}_2$ -0.5 films shown in Fig. 2e revealed that the characteristic peaks for Ti, O, Bi and Se were marked with atomic percentages of Bi and Se of 0.9% and 1.3%, respectively. It is well known that the measurement error of EDS test is increased with the decrease of content of test element. So, it is acceptable that the atomic ratio of Bi and Se is close to 2:3.

Figure 3a shows the XRD spectra for pure TiO_2 (curve a) and $\text{Bi}_2\text{Se}_3/\text{TiO}_2$ -1.0 nanocomposites (curve b). Aside from the Ti substrate peaks, the diffraction peaks at 25.38° , 38.03° , 48.01° , 54.05° , 55.17° , 62.71° and 70.44° were well matched with the lattice planes (101), (004), (200), (105), (211), (204) and (220) of anatase TiO_2 , respectively (JCPDS 21-1272). Except for the TiO_2 peaks, the distinctive diffraction peaks at 29.35° and 74.90° were indexed to the lattice planes (015) and (0216) of the rhombohedral crystal Bi_2Se_3 (JCPDS 33-0214). However, there is no obvious peak of $\text{Bi}_2\text{Se}_3/\text{TiO}_2$ -1.0 due to low content Bi_2Se_3 deposited on TiO_2 and the XRD spectra conformed to the SEM and EDS results. X-ray photoelectron spectroscopy (XPS) was used to further determine the chemical compositions and states of the $\text{Bi}_2\text{Se}_3/\text{TiO}_2$ nanocomposites. As shown in Fig. 3b, XPS revealed the existence of Bi, Se, Ti and O components in addition to C contaminants due to adventitious hydrocarbon contamination. Figure 3c shows the peak positions for Ti 2p at 458.7 and 464.5 eV, indicating that the titanium oxides mainly consisted of TiO_2 [52]. As illustrated in Fig. 3d, the O 1s semaphores matched with two Gaussian peaks: the maximum at the lower binding energy (530.0 eV) was attributed to the lattice oxygen (O_L) in $\text{Bi}_2\text{Se}_3/\text{TiO}_2$ nanocomposites and the second at the higher binding energy (531.5 eV) was derived from the adsorbed oxygen (O_A), including weak bonding oxygen or hydroxyl groups. The existence of O_A was due to the generation of oxygen vacancies on the surface of the nanocomposites, which might improve the photoelectric



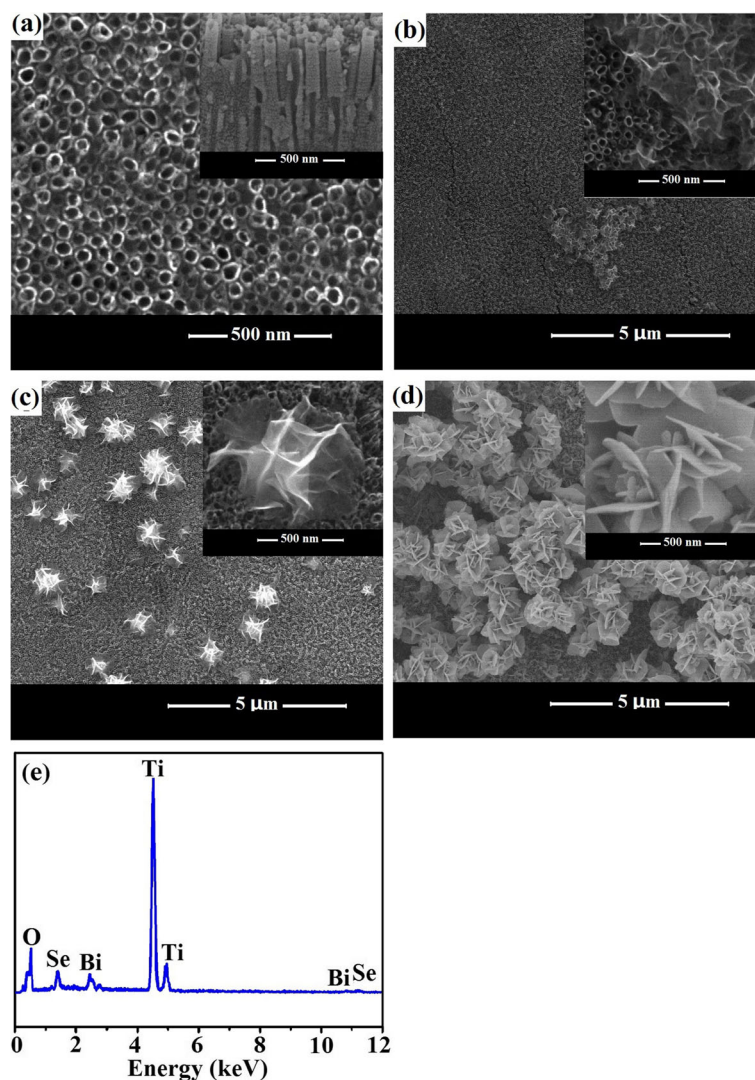


Fig. 2 SEM images for **a** pure TiO_2 , **b** $\text{Bi}_2\text{Se}_3/\text{TiO}_2$ -0.25, **c** $\text{Bi}_2\text{Se}_3/\text{TiO}_2$ -0.5 and **d** $\text{Bi}_2\text{Se}_3/\text{TiO}_2$ -1.0; **e** EDS spectrum for $\text{Bi}_2\text{Se}_3/\text{TiO}_2$ -0.5 films

conversion properties of $\text{Bi}_2\text{Se}_3/\text{TiO}_2$ nanocomposites in photocathodic protection [53]. Figure 3e shows that the $4f_{7/2}$ asymmetric peak for Bi resolved into two peaks (157.5 and 159.4 eV), with the Bi $4f_{5/2}$ spectrum similarly divided into two bands at 162.8 and 164.7 eV, respectively. The positions of the lower peaks (157.5 eV and 162.8 eV) were in good agreement with those in Bi_2Se_3 , with the higher peaks corresponding to bismuth oxide at 159.4 eV and 164.7 eV [54, 55]. It can be concluded that a handful of bismuth metal was oxidized during the synthetic process with Bi_2Se_3 modifying pure TiO_2 . As shown in Fig. 3f, the two peaks were assigned to the $3d_{3/2}$ and $3d_{5/2}$ core levels of Se at 55.1 and 54.2 eV, respectively, indicating that Se existed in the form of Se^{2-} [56].

Figure 4 shows the light absorption abilities of pure TiO_2 and $\text{Bi}_2\text{Se}_3/\text{TiO}_2$ -1.0 nanocomposites. The characteristic absorption edge for pure TiO_2 was approximately

380 nm within the UV region due to the bandgap energy of anatase TiO_2 (3.2 eV) (curve a). Pronounced adsorption was observed for $\text{Bi}_2\text{Se}_3/\text{TiO}_2$ nanocomposites in the visible light region (350–800 nm) (curve b), with visible light absorption abilities higher than those of pure TiO_2 due to the incorporation of the Bi_2Se_3 nanoflower. This phenomenon can be ascribed to the fact that Bi_2Se_3 is excited under visible light due to its narrow bandgap (0.35 eV), with electrons and holes produced in its conduction band (CB) and valence band (VB). Therefore, the addition of Bi_2Se_3 effectively increases the visible light absorption capability of $\text{Bi}_2\text{Se}_3/\text{TiO}_2$ nanocomposites.

Photocathodic Protection Performance of Pure TiO_2 and $\text{Bi}_2\text{Se}_3/\text{TiO}_2$

As shown in Fig. 5, the OCP curves for 304ss coupled with pure TiO_2 and $\text{Bi}_2\text{Se}_3/\text{TiO}_2$ nanocomposite photoanodes

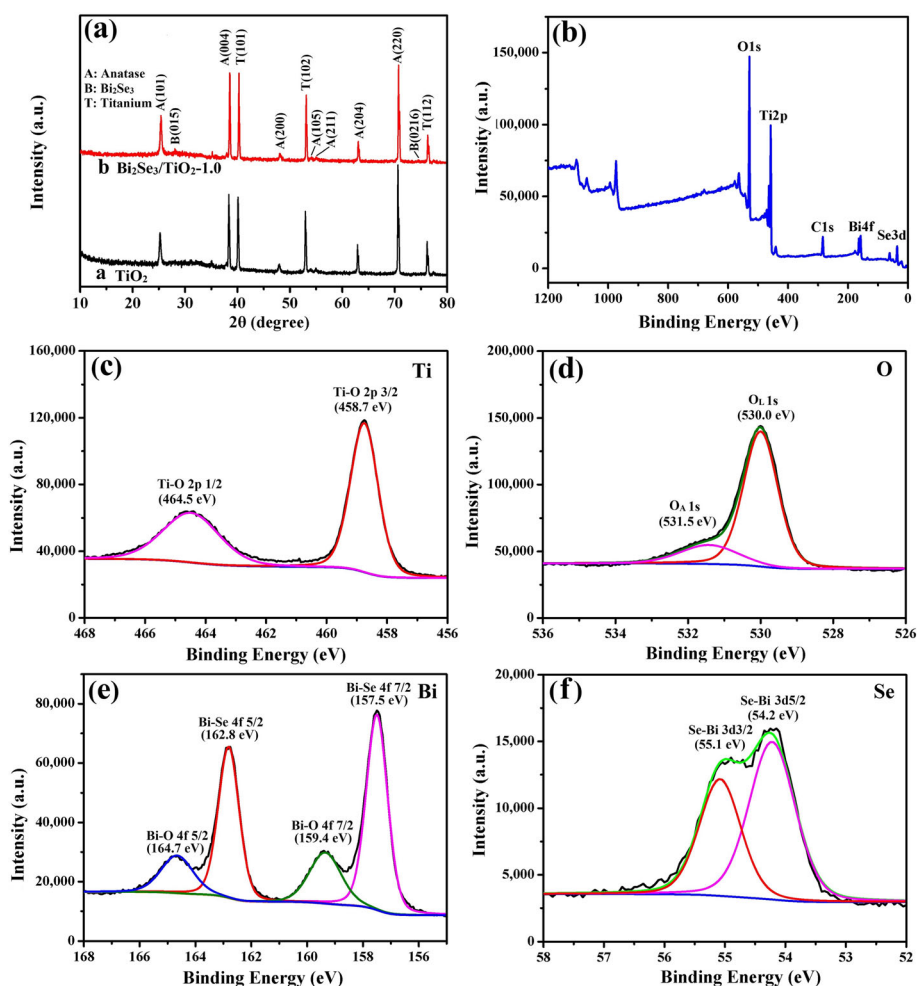


Fig. 3 a XRD patterns for pure TiO_2 and $\text{Bi}_2\text{Se}_3/\text{TiO}_2$ -1.0 nanocomposites; b the total survey spectrum, c Ti 2p, d O 1s, e Bi 4f and f Se 3d XPS spectra for $\text{Bi}_2\text{Se}_3/\text{TiO}_2$ -1.0 nanocomposites

were measured under intermittent visible light, with the OCP response to illumination prompted and shifted to a negative potential for all of the coupled electrodes. At the initial phase of light on, the OCP for all of the coupled electrodes showed a negative shift over a short time, which was due to the transfer of the excited photoelectrons from the pure TiO_2 and $\text{Bi}_2\text{Se}_3/\text{TiO}_2$ nanocomposite to the 304ss electrode [1, 57]. Subsequently, the relatively stable OCP values can be attributed to the balancing rate between the creation and recombination of photogenerated electrons [32]. After switching off the irradiation, the OCP values for the $\text{Bi}_2\text{Se}_3/\text{TiO}_2$ nanocomposites returned to their original values at a slower speed compared to pure TiO_2 . This phenomenon might be attributed to the electron pool effect of $\text{Bi}_2\text{Se}_3/\text{TiO}_2$ nanocomposites, which can store photoinduced electrons under light irradiation and slowly release these electrons without light irradiation. Under visible light irradiation, the OCP value for 304ss was approximately -450 mV when coupled with TiO_2

(curve a), and the OCP values for 304ss coupled with $\text{Bi}_2\text{Se}_3/\text{TiO}_2$ -0.25 (curve b), $\text{Bi}_2\text{Se}_3/\text{TiO}_2$ -0.5 (curve d) and $\text{Bi}_2\text{Se}_3/\text{TiO}_2$ -1.0 (curve c) reached -905 mV, -996 mV and -958 mV, respectively. These results indicated that 304ss was cathodically polarized once coupled with $\text{Bi}_2\text{Se}_3/\text{TiO}_2$ nanocomposites and that a good cathodic protection for 304ss might be provided by the $\text{Bi}_2\text{Se}_3/\text{TiO}_2$ photoanodes. As shown in Fig. 5 d, the 304ss coupled to $\text{Bi}_2\text{Se}_3/\text{TiO}_2$ -0.5 possessed most negative potential indicated that the best photocathodic protection performance for 304ss. This result might be because the active sites and light harvesting increased with the increasing Bi_2Se_3 content. However, an excessive amount of Bi_2Se_3 particles served as the recombination sites for electrons and holes, which hindered the charge transfer from the $\text{Bi}_2\text{Se}_3/\text{TiO}_2$ nanocomposites to 304ss.

As shown in Fig. 6, the photocurrent density vs. time curves for TiO_2 and $\text{Bi}_2\text{Se}_3/\text{TiO}_2$ nanocomposites showed a rapid and reproducible photoresponse under

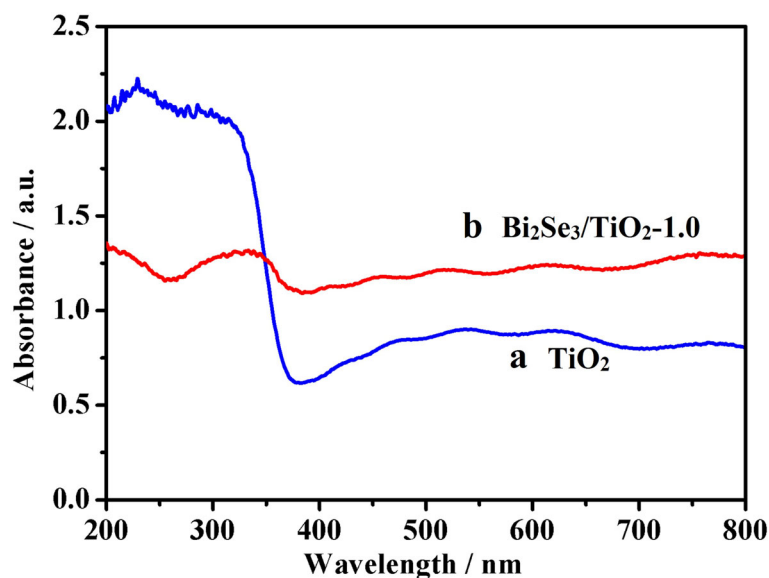


Fig. 4 UV-visible absorption spectra for TiO₂ (a) and Bi₂Se₃/TiO₂-1.0 (b)

intermittent visible light illumination, which reflected the photoelectric conversion performance of the materials. The photogenerated current was relatively small under visible light due to weak visible light absorption (curve a). However, the photogenerated current increased remarkably under visible light illumination following sensitization of TiO₂ by the Bi₂Se₃ nanoflower (curves b to d). The data implied that the Bi₂Se₃/TiO₂ nanocomposites were capable of utilizing visible light and that the heterojunction between TiO₂ and Bi₂Se₃ promoted the separation of photogenerated electrons and holes [58]. Furthermore, the photoelectrons produced in the conduction band of the Bi₂Se₃ nanoflower

can be easily transferred to the more positive conduction band of the TiO₂ nanotubes under visible light illumination. After three irradiation interval, the photocurrent maintained a relatively steady value and no photocurrent degradation was detected, illustrating the good photochemical stability of the Bi₂Se₃/TiO₂ nanocomposite films. For different concentrations of Bi³⁺, the Bi₂Se₃/TiO₂ nanocomposites showed different intensities for the photocurrent response. In particular, the transient photocurrent density for Bi₂Se₃/TiO₂-0.5 (415 $\mu\text{A}/\text{cm}^2$) was higher than that for Bi₂Se₃/TiO₂-0.25 (85 $\mu\text{A}/\text{cm}^2$) and Bi₂Se₃/TiO₂-1.0 (160 $\mu\text{A}/\text{cm}^2$), indicating that Bi₂Se₃/TiO₂-0.5 possessed an ideal separation efficiency

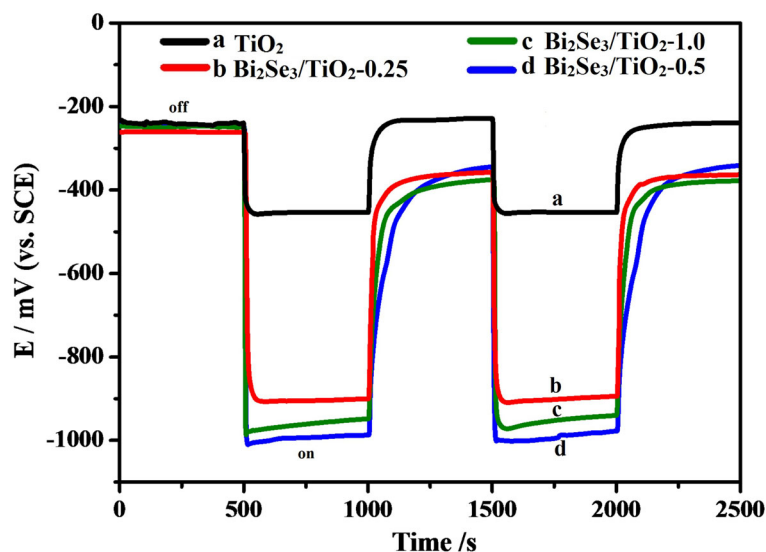


Fig. 5 OCP for 304ss coupled with pure TiO₂ and Bi₂Se₃/TiO₂ nanocomposites in a 0.5 mol NaCl solution

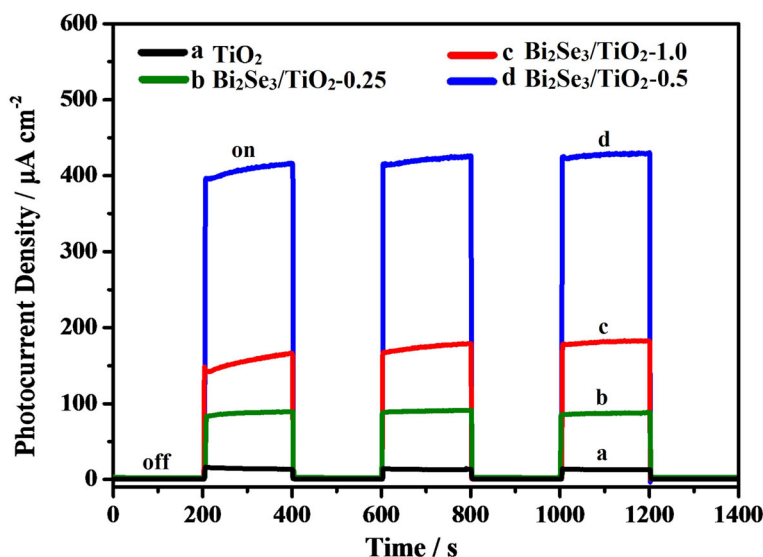


Fig. 6 Photocurrent density vs. time curves for pure TiO_2 and $\text{Bi}_2\text{Se}_3/\text{TiO}_2$ nanocomposites in 0.1 mol/L Na_2S and 0.2 mol/L NaOH mixed solution

for the photogenerated electron-hole pairs. The active sites and light harvesting were decreased because of the deficiency of Bi_2Se_3 nanoflowers on the $\text{Bi}_2\text{Se}_3/\text{TiO}_2$ nanocomposite films, while recombination sites for electrons and holes increased in the presence of an excessive amount of Bi_2Se_3 nanoflowers. Under visible light illumination, the largest photoinduced current density of the $\text{Bi}_2\text{Se}_3/\text{TiO}_2-0.5$ photoanode was consistent with the largest photoinduced potential drops illustrated in Fig. 5, further validating the optimal photocathodic protection performance of $\text{Bi}_2\text{Se}_3/\text{TiO}_2-0.5$ for 304ss.

Figure 7 shows the photoelectric conversion and transportation processes for the $\text{Bi}_2\text{Se}_3/\text{TiO}_2$ nanocomposites. Under visible light, Bi_2Se_3 nanoflowers can readily

absorb photons as they contain adsorbed oxygen (O_A) and have a narrow bandgap width (0.35 eV). When the photons are absorbed by the Bi_2Se_3 nanoflowers, photoexcited electrons will be generated by excitation from the valence band (VB) of Bi_2Se_3 to the conduction band (CB) of Bi_2Se_3 . The photoexcited electrons in the CB of Bi_2Se_3 are shifted to the CB of TiO_2 , while the photo-generated holes in the VB of TiO_2 are transferred to the VB of Bi_2Se_3 , and then are captured by S^{2-} in the electrolyte to turn into S on the surface of photoanode film. When the photoexcited electrons exit the photoanode and transfer to 304ss, they will react with the oxygen gas and water to convert OH^- . Furthermore, Na^+ is transported from electrolytic cell to photolysis cell by proton

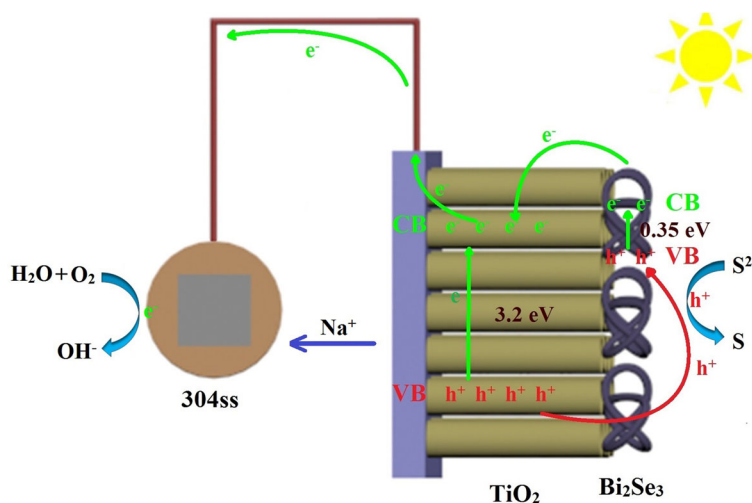


Fig. 7 Schematic representation of the electron transfer processes in $\text{Bi}_2\text{Se}_3/\text{TiO}_2$

exchange membrane, so that the coupling system is electrically neutral as a whole. As a consequence, the photogenerated charges are effectively separated and the recombination probability for photogenerated electron-hole pairs is reduced. Once 304ss receives photoexcited electrons from the $\text{Bi}_2\text{Se}_3/\text{TiO}_2$ nanocomposite through the wire, the potential of 304ss shifts negatively. Under visible light illumination, the $\text{Bi}_2\text{Se}_3/\text{TiO}_2$ nanocomposites can reduce the corrosion rate of 304ss. Therefore, the efficient separation of photo-excited electron-hole pairs in $\text{Bi}_2\text{Se}_3/\text{TiO}_2$ nanocomposites will accelerate the redox reaction and generate effective photocathodic protection for 304ss.

Conclusions

In this paper, TiO_2 nanotube arrays were prepared by the anodization method and Bi_2Se_3 nanoflowers were grown on TiO_2 nanotubes by chemical bath deposition. The $\text{Bi}_2\text{Se}_3/\text{TiO}_2$ nanocomposites showed a homogeneous distribution and ordered characteristics. Electrochemical tests for the nanocomposites and pure TiO_2 coupled with 304ss showed that the photogenerated cathodic protection performance of the $\text{Bi}_2\text{Se}_3/\text{TiO}_2$ nanocomposites was superior compared to that for pure TiO_2 . The OCP value for 304ss coupled with $\text{Bi}_2\text{Se}_3/\text{TiO}_2$ -0.5 showed a negative shift to -996 mV under visible light illumination due to the active sites and light harvesting of TiO_2 sensitized by Bi_2Se_3 . By comparing the results of the electrochemical tests for three $\text{Bi}_2\text{Se}_3/\text{TiO}_2$ nanocomposites, the nanocomposite prepared using 0.5 mmol/L Bi^{3+} in the electrolyte exhibited optimal performance.

Abbreviations

304ss: 304 stainless steel; CB: Conduction band; CE: The counter electrode; EDS: Energy-dispersive X-ray spectroscopy; H_3NTA : Nitrilotriacetic acid; OA: Adsorbed oxygen; OCP: Open-circuit potential; OL: Lattice oxygen; RE: The reference electrode; SCE: Saturated calomel electrode; SEM: Scanning electron microscopy; UV-Vis: UV-visible diffuse reflectance spectra; VB: Valence band; WE: The working electrode; XPS: X-ray photoelectron spectroscopy; XRD: X-ray diffraction

Funding

This work is supported by the Project of CAS Strategic Priority Project (XDA13040404), Shandong Key Research and Development Program (2016GGH4511), and NSFC (No. U1660112).

Availability of Data and Materials

All datasets are presented in the main paper.

Authors' Contributions

WCW performed the synthesis and characterization of $\text{Bi}_2\text{Se}_3/\text{TiO}_2$ films. XTW, NW and XBN took part in the synthesis. DZL, XJL and QCZ participated in the characterization. WCW supervised the conceptual framework and drafted the manuscript. HL, XTW and YLH were participants in writing the manuscript. All authors read and approved the final manuscript.

Authors' Information

XTW is a research professor and master supervisor in the Institute of Oceanology, Chinese Academy of Sciences (IOCAS). YLH is a research professor and doctor supervisor in the IOCAS. DZL and NW are research assistants in the IOCAS. HL is a lecturer in the Qingdao University. WCW, XJL and QCZ are doctorate candidates in the IOCAS. XBN is a graduate in the Qingdao National Laboratory for Marine Science and Technology.

Ethics Approval and Consent to Participate

Not applicable.

Consent for Publication

Not applicable.

Competing Interests

The authors declare that they have no competing interests.

Publisher's Note

Springer Nature remains neutral with regard to jurisdictional claims in published maps and institutional affiliations.

Author details

¹Key Laboratory of Marine Environmental Corrosion and Bio-fouling, Institute of Oceanology, Chinese Academy of Sciences, 7 Nanhai Road, Qingdao 266071, China. ²Open Studio for Marine Corrosion and Protection, Pilot National Laboratory for Marine Science and Technology, Qingdao 266237, China. ³University of Chinese Academy of Sciences, Beijing 100049, China. ⁴College of Mechanical and Electrical Engineering, Qingdao University, Qingdao 266071, China. ⁵Center for Ocean Mega-Science, Chinese Academy of Sciences, Qingdao 266071, China.

Received: 11 July 2018 Accepted: 13 September 2018

Published online: 21 September 2018

References

- Lin ZQ, Lai YK, Hu RG et al (2010) A highly efficient $\text{ZnS}/\text{CdS}/\text{TiO}_2$ photoelectrode for photogenerated cathodic protection of metals. *Electrochim Acta* 55:8717–8723
- Ryan MP, Williams DE, Chater RJ et al (2002) Why stainless steel corrodes. *Nature* 415:770–774
- Robertson J (1991) The mechanism of high-temperature aqueous corrosion of stainless-steels. *Corros Sci* 32:443–465
- Hou B, Li X, Ma X et al (2017) The cost of corrosion in China. *Npj Mater Degr* 1:1–10
- Abdulagatov AI, Yan Y, Cooper JR et al (2011) Al_2O_3 and TiO_2 atomic layer deposition on copper for water corrosion resistance. *ACS Appl Mater Interfaces* 3:4593–4601
- Gonzalez MB, Saidman SB (2011) Electrodeposition of polypyrrole on 316L stainless steel for corrosion prevention. *Corros Sci* 53:276–282
- Jingling MA, Jiuba W, Gengxin LI et al (2010) The corrosion behaviour of Al-Zn-In-Mg-Ti alloy in NaCl solution. *Corros Sci* 52:534–539
- Glass GK, Hassanein AM, Buenfeld NR (2001) Cathodic protection afforded by an intermittent current applied to reinforced concrete. *Corros Sci* 43: 1111–1131
- Kear G, Barker BD, Stokes KR et al (2005) Corrosion and impressed current cathodic protection of copper-based materials using a bimetallic rotating cylinder electrode (BRCE). *Corros Sci* 47:1694–1705
- Yuan J (1995) Characterization of sol-gel-derived TiO_2 coatings and their photoeffects on copper substrates. *J Electrochem Soc* 142:3444–3450
- Subasri R, Shinohara T, Mori K (2005) Modified TiO_2 coatings for cathodic protection applications. *Sci Technol Adv Mat* 6:501–507
- Lei CX, Feng ZD, Zhou H (2012) Visible-light-driven photogenerated cathodic protection of stainless steel by liquid-phase-deposited TiO_2 films. *Electrochim Acta* 68:134–140
- Zhang W, Guo H, Sun H et al (2017) Constructing ternary polyaniline-graphene- TiO_2 hybrids with enhanced photoelectrochemical performance in photo-generated cathodic protection. *Appl Surf Sci* 410:547–556
- Cui S, Yin X, Yu Q et al (2015) Polypyrrole nanowire/ TiO_2 nanotube nanocomposites as photoanodes for photocathodic protection of Ti substrate and 304 stainless steel under visible light. *Corros Sci* 98:471–477
- Zhang LW, Fu HB, Zhu YF (2008) Efficient TiO_2 photocatalysts from surface hybridization of TiO_2 particles with graphite-like carbon. *Adv Funct Mater* 18:2180–2189
- Liu B, Aydil ES (2009) Growth of oriented single-crystalline rutile TiO_2 nanorods on transparent conducting substrates for dye-sensitized solar cells. *J Am Chem Soc* 131:3985–3990
- Tang H, Prasad K, Sanjines R et al (1995) TiO_2 anatase thin-films as gas sensors. *Sensors Actuat B-Chem* 26:71–75

18. Yang Y, Cheng YF (2017) Bi-layered $\text{CeO}_2/\text{SrTiO}_3$ nanocomposite photoelectrode for energy storage and photocathodic protection. *Electrochim Acta* 253:134–141
19. Liu Q, Hu J, Liang Y et al (2016) Preparation of $\text{MoO}_3/\text{TiO}_2$ composite films and their application in photoelectrochemical anticorrosion. *J Electrochem Soc* 163:C539–CC44
20. Zhang J, Hu J, Zhu YF et al (2015) Fabrication of CdTe/ZnS core/shell quantum dots sensitized TiO_2 nanotube films for photocathodic protection of stainless steel. *Corros Sci* 99:118–124
21. Li H, Wang X, Zhang L et al (2015) CdTe and graphene co-sensitized TiO_2 nanotube array photoanodes for protection of 304ss under visible light. *Nanotechnology* 26:155704
22. Li H, Wang X, Liu Y et al (2014) Ag and SnO_2 co-sensitized TiO_2 photoanodes for protection of 304ss under visible light. *Corros Sci* 82:145–153
23. Gao T, Chen Z, Niu F et al (2015) Shape-controlled preparation of bismuth ferrite by hydrothermal method and their visible-light degradation properties. *J Alloy Compd* 648:564–570
24. Li J, Lin CJ, Lai YK et al (2010) Photogenerated cathodic protection of flower-like, nanostructured, N-doped TiO_2 film on stainless steel. *Surf Coat Tech* 205:557–564
25. Arman SY, Omidvar H, Tabaian SH et al (2014) Evaluation of nanostructured S-doped TiO_2 thin films and their photoelectrochemical application as photoanode for corrosion protection of 304 stainless steel. *Surf Coat Tech* 251:162–169
26. Kim Y, Yang S, Jeon E et al (2004) Enhancement of photo-oxidation activities depending on structural distortion of Fe-doped TiO_2 nanoparticles. *Nanoscale Res Lett* 11:41
27. Sanjabi S, Shirani A (2012) The morphology and corrosion resistance of electrodeposited Co-TiO_2 nanocomposite coatings. *Mater Corros* 63:695–702
28. Obregón S, Muñoz-Batista MJ, Fernández-García M et al (2015) Cu-TiO_2 systems for the photocatalytic H_2 production: influence of structural and surface support features. *Appl Catal B-Environ* 179:468–478
29. Li SN, Wang Q, Chen T et al (2012) Study on cerium-doped nano- TiO_2 coatings for corrosion protection of 316 L stainless steel. *Nanoscale Res Lett* 7:277
30. Hu XL, Liu X, Tian J et al (2017) Towards full-spectrum (UV, visible, and near-infrared) photocatalysis: achieving an all-solid-state Z-scheme between Ag_2O and TiO_2 using reduced graphene oxide as the electron mediator. *Catal Sci Technol* 7:4193–4205
31. Zhang L, Wang XT, Liu FG et al (2015) Photogenerated cathodic protection of 304ss by ZnSe/TiO_2 NTs under visible light. *Mater Lett* 143:116–119
32. Zhou MJ, Zeng ZO, Zhong L (2009) Photogenerated cathode protection properties of nano-sized TiO_2/WO_3 coating. *Corros Sci* 51:1386–1391
33. Jang JS, Ji SM, Bae SW et al (2007) Optimization of CdS/TiO_2 nano-bulk composite photocatalysts for hydrogen production from $\text{Na}_2\text{S}/\text{Na}_2\text{SO}_3$ aqueous electrolyte solution under visible light ($\lambda \geq 420$ nm). *J Photoch Photobio A* 188:112–119
34. Ning XB, Ge SS, Wang XT et al (2017) Preparation and photocathodic protection property of $\text{Ag}_2\text{S-TiO}_2$ composites. *J Alloy Compd* 719:15–21
35. Liu Y, Zhao L, Li MT et al (2014) TiO_2/CdSe core-shell nanofiber film for photoelectrochemical hydrogen generation. *Nanoscale* 6:7397–7404
36. Hu J, Guan ZC, Liang Y et al (2017) Bi_2Se_3 modified single crystalline rutile TiO_2 nanorod array films for photoelectrochemical cathodic protection. *Corros Sci* 125:59–67
37. Hasan MZ, Kane CL (2010) Colloquium: topological insulators. *Rev Mod Phys* 82:3045–3067
38. Sun ZL, Liufu SC, Chen LD (2010) Synthesis and characterization of nanostructured bismuth selenide thin films. *Dalton T* 39:10883–10887
39. Sun ZL, Liufu SC, Chen XH et al (2010) Enhancing thermoelectric performance of bismuth selenide films by constructing a double-layer nanostructure. *Crystengcomm* 12:2672–2674
40. Waters J, Crouch D, Raftery J et al (2004) Deposition of bismuth chalcogenide thin films using novel single-source precursors by metal-organic chemical vapor deposition. *Chem Mater* 16:3289–3298
41. Kharade SD, Pawar NB, Ghanwat VB et al (2013) Room temperature deposition of nanostructured Bi_2Se_3 thin films for photoelectrochemical application: effect of chelating agents. *New J Chem* 37:2821–2828
42. Desai ND, Ghanwat VB, Khot KV et al (2016) Effect of substrate on the nanostructured Bi_2Se_3 thin films for solar cell applications. *J Mater Sci-Mater El* 27:2385–2393
43. Braun L, Mussler G, Hruban A et al (2016) Ultrafast photocurrents at the surface of the three-dimensional topological insulator Bi_2Se_3 . *Nat Commun* 7:13259
44. Liu C, Zhang HB, Sun Z et al (2016) Topological insulator Bi_2Se_3 nanowire/Si heterostructure photodetectors with ultrahigh responsivity and broadband response. *J Mater Chem C* 4:5648–5655
45. Alegria LD, Petta JR (2012) Controlled MOCVD growth of Bi_2Se_3 topological insulator nanoribbons. *Nanotechnology* 23:435601
46. Knebl GM, Gessler JR, Kamp M et al (2014) Molecular beam epitaxial growth of Bi_2Se_3 nanowires and nanoflakes. *Appl Phys Lett* 105:226801
47. Zhu H, Richter CA, Zhao EH et al (2013) Topological insulator Bi_2Se_3 nanowire high performance field-effect transistors. *Sci Rep-UK* 3:1757
48. Onose Y, Yoshimi R, Tsukazaki A et al (2011) Pulsed laser deposition and ionic liquid gate control of epitaxial Bi_2Se_3 thin films. *Appl Phys Express* 4:083001
49. Cha JJ, Claassen M, Kong DS et al (2012) Effects of magnetic doping on weak antilocalization in narrow Bi_2Se_3 nanoribbons. *Nano Lett* 12:4355–4359
50. Raja KS, Gandhi T, Misra M (2007) Effect of water content of ethylene glycol as electrolyte for synthesis of ordered titania nanotubes. *Electrochem Commun* 9:1069–1076
51. Hensel J, Wang GM, Li Y et al (2010) Synergistic effect of CdSe quantum dot sensitization and nitrogen doping of TiO_2 nanostructures for photoelectrochemical solar hydrogen generation. *Nano Lett* 10:478–483
52. Wu Q, Ouyang JJ, Xiea KP et al (2012) Ultrasound-assisted synthesis and visible-light-driven photocatalytic activity of Fe-incorporated TiO_2 nanotube array photocatalysts. *J Hazard Mater* 199:410–417
53. Li H, Wang X, Wei Q et al (2017) Photocathodic protection of 304 stainless steel by $\text{Bi}_2\text{S}_3/\text{TiO}_2$ nanotube films under visible light. *Nanoscale Res Lett* 12:80
54. Kong DS, Cha JJ, Lai KJ et al (2011) Rapid surface oxidation as a source of surface degradation factor for Bi_2Se_3 . *ACS Nano* 5:4698–4703
55. Dharmadhikari VS, Sainkar SR, Badrinarayan S et al (1982) Characterization of thin-films of bismuth oxide by X-ray photo-electron spectroscopy. *J Electron Spectrosc* 25:181–189
56. Nascimento VB, Carvalho VE, Paniago R et al (1999) XPS and EELS study of the bismuth selenide. *J Electron Spectrosc* 104:99–107
57. Lei C, Liu Y, Zhou H et al (2013) Photogenerated cathodic protection of stainless steel by liquid-phase-deposited sodium polyacrylate/ TiO_2 hybrid films. *Corros Sci* 68:214–222
58. Liu CJ, Yang Y, Li WZ et al (2016) A novel Bi_2S_3 nanowire @ TiO_2 nanorod heterogeneous nanostructure for photoelectrochemical hydrogen generation. *Chem Eng J* 302:717–724

Submit your manuscript to a SpringerOpen[®] journal and benefit from:

- Convenient online submission
- Rigorous peer review
- Open access: articles freely available online
- High visibility within the field
- Retaining the copyright to your article

Submit your next manuscript at ► springeropen.com